HHS Public Access

Lysophosphatidic Acid Increases Maturation of Brush Borders and SGLT1 activity in MYO5B-deficient Mice, a Model of Microvillus Inclusion Disease

Izumi Kaji[1,2,†], **Joseph T. Roland**[1,2], **Masahiko Watanabe**[4], **Amy C. Engevik**[1,2], **Anna E. Goldstein**[1,2], **Craig A. Hodges**[5], **James R. Goldenring**[1,2,3,6]

[1]Section of Surgical Sciences, Vanderbilt University Medical Center, Sapporo, Japan

[2]Epithelial Biology Center, Vanderbilt University School of Medicine, Sapporo, Japan

[3]Cell and Developmental Biology, Vanderbilt University School of Medicine, Sapporo, Japan

[4]Hokkaido University Graduate School of Medicine, Sapporo, Japan

[5]Cystic Fibrosis Mouse Models Resource Center, Case Western Reserve University, Cleveland, OH

[6]Nashville Veterans Affairs Medical Center, Nashville TN

Abstract

Background & Aim: Myosin VB (MYO5B) is an essential trafficking protein for membrane recycling in gastrointestinal epithelial cells. The inactivating mutations of MYO5B cause the congenital diarrheal disease, microvillus inclusion disease (MVID). MYO5B deficiency in mice causes mislocalization of SGLT1 and NHE3, but retained apical function of CFTR, resulting in malabsorption and secretory diarrhea. Activation of lysophosphatidic acid (LPA) receptors can improve diarrhea, but the effect of LPA on MVID symptoms is unclear. We investigated whether LPA administration can reduce the epithelial deficits in MYO5B-knockout mice.

Methods: Studies were conducted with tamoxifen-induced, intestine-specific knockout of MYO5B (*VilCre*[ERT2];*Myo5b*[flox/flox]) and littermate controls. Mice were given LPA, an LPAR2

agonist (GRI977143), or vehicle for 4 days after a single injection of tamoxifen. Apical SGLT1 and CFTR activities were measured in Üssing chambers. Intestinal tissues were collected, and localization of membrane transporters was evaluated by immunofluorescence analysis in tissue sections and enteroids. RNA sequencing and enrichment analysis were performed with isolated jejunal epithelial cells.

Results: Daily administration of LPA reduced villus blunting, frequency of multivesicular bodies and levels of cathepsins in intestinal tissues of MYO5B-knockout mice compared to vehicle administration. LPA partially restored the brush border height and the localization of SGLT1 and NHE3 in small intestine of MYO5B-knockout mice and enteroids. The SGLT1-dependent short-circuit current was increased and abnormal CFTR activities were decreased in jejunum from MYO5B-knockout mice given LPA compared with vehicle.

Conclusions: LPA may regulate a MYO5B-independent trafficking mechanism and brush border maturation, and therefore be developed for treatment of MVID.

Keywords

G protein-coupled receptors; nutrient absorption; digital image analysis

Introduction

Lysophosphatidic acid (LPA) is present in food plants[1] and in mammalian organs, and is synthesized in the serum at sub-micromolar levels, functioning as a growth factor-like phospholipid.[2–4] Several phospholipases (PLs), such as PLA_1, PLA_2, PLD, and autotaxin derive LPA from phosphatidic acid or other lysophospholipids in a variety of tissues, including the gastrointestinal tract.[5] LPA is known to activate the G protein-coupled receptors LPAR1–6, GPR35, and GPR87.[6] Although the distribution of each receptor protein has not been clarified, mRNA expressions of *Lpar1, Lpar2,* and *Lpar3* have been detected in enterocytes and dominant expression of *Lpar5* in the stem cells of mouse intestine, and *LPAR1* and *LPAR5* are major LPA receptors in human small intestine.[7–9] Work with transgenic mice previously demonstrated that LPAR2 activation inhibited the cystic fibrosis transmembrane conductance regulator (CFTR)-dependent secretory diarrhea that is induced by cholera toxin,[10] while activation of LPAR5 stimulated the trafficking of the sodium-proton exchanger NHE3 (also known as Slc9a3) that enhances water absorption. [11] A recent study with mouse enteroids showed that the supplementation of medium with LPA, instead of epidermal growth factor, enhanced the proliferation and differentiation of these enteroids via the LPAR1.[4] Based on these studies, we hypothesized that multiple LPA signaling pathways are important for intestinal epithelial cell functions, and that the exogenous LPA may alleviate some epithelial defects that are seen in congenital diarrheal diseases.

Myosin Vb (MYO5B) is an essential trafficking protein for membrane recycling in gastrointestinal epithelial cells and its inhibition through truncation or missense mutations causes the congenital diarrheal disorder, microvillus inclusion disease (MVID).[12, 13] Autosomal recessive MVID is characterized by feeding-induced dehydrating diarrhea usually starting in the first week after birth, correlating with villus blunting, loss of

microvilli on the apical membrane, loss of apical sodium transporters NHE3 and SGLT1 from the brush border, formation of intracellular inclusions containing microvilli, and the presence of large autophagic lysosomes.[14, 15] *VilCre^ERT2;Myo5b^flox/flox* mice represent a model for the intestinal pathophysiology observed in MVID patients and survive no longer than 4 days after tamoxifen-induced MYO5B deletion.[16, 17] We recently reported that either germline or enterocyte-specific MYO5B deficiency in mice causes immature brush border formation, ezrin-positive microvillus inclusions, mis-localization of the sodium-glucose cotransporter SGLT1 and NHE3, but retains stable expression of CFTR on the apical membrane.[18] SGLT1 is an essential apical transporter for glucose/galactose absorption, as well as sodium and water absorption in the small intestine.[19, 20] Consistent with the observed patterns of apical protein localization, induced adult MYO5B-knockout mice show decreased functional SGLT1 and increased CFTR activity in jejunal and ileal mucosa mounted in the Üssing chamber trans-mucosal ion transport measurement system.[18] The resulting hypersecretion of water and malabsorption of sodium recorded in this assay mimics the malabsorption and life-threatening watery diarrhea that is the hallmark of MVID. Presently, continuous total parental nutrition therapy or intestinal transplantation are the only options for sustaining MVID patients. In this study we evaluated the therapeutic potential of LPA on intestinal epithelial cell function in an MVID model of inducible intestinal MYO5B-knockout mice.

Materials and Methods

Chemicals

LPA (18:1 Lyso PA; 857231-P) was purchased from Avanti Polar Lipids and dissolved in sterile PBS containing 0.1% fatty acid-free BSA (A6003, Sigma). Aliquots of LPA were stored in glass vials at −20°C. GRI-977143 was purchased from Cayman Chemical (Ann Arbor, MI). (R)-BPO-27 was from MedChem Express (Monmouth Junction, NJ). All other chemicals not specified were purchased from Sigma.

Animals

The Institutional Animal Care and Use Committee (IACUC) of Vanderbilt University Medical Center approved all experimental procedures and animal care. *In vivo* experiments were described according to the Animal Research: Reporting of In Vivo Experiments (ARRIVE) checklist. All animals that were used in this study were housed in groups of 3–5 mice, fed standard pellet diet with water *ad libitum*, under a 12-hour light/dark cycle in a specific pathogen free facility. *VilCre^ERT2;Myo5b^flox/flox* mice with C57BL/6 background were generated and Cre recombinase was activated at the age of 8–12 weeks (day 0) with a single dose of tamoxifen, as previously reported.[17] LPAR agonists were given at 1600 for 4 days from the day of tamoxifen induction. LPA (3 mg/kg) was administered by oral gavage (og) or intraperitoneal (ip) injection, and an LPAR2 agonist GRI-977143 (3 mg/kg) was injected ip. Tamoxifen-injected *VilCre^ERT2;Myo5b^fox/−* or *Myo5b^flox/flox* mice were used as control. On day 4, mice were euthanized, and samples were collected. The entire small intestine was collected for immunohistochemical and image analysis. A piece of jejunum (approximately 8–11 cm from the pyloric ring) from mice was used for Üssing chamber

measurements or RNA sequencing (RNA-seq; supplemental methods). The number of animals were specified in each result.

Antibody production

Antibodies were produced in accordance with the Guidelines for the Care and Use of Laboratory Animals of the Hokkaido University. Affinity-purified polyclonal antibodies were raised against recombinant peptides of mouse SGLT1 (NP_062784.3; amino acid residues 576-610) and of mouse CFTR (NP_066388.1; 634–675 and 1438–1476), respectively, using the same method as described previously.[21] Specificity of each antibody was confirmed by immunostaining in *Sglt1*-knockout (a gift from Dr. Koepsell)[22] or *Cftr* null (G542X mutation generated in Case Western CF Mouse Model Core)[23] mouse tissues (Supplemental Figures 1 and 2).

Immunofluorescence staining and imaging

Intestinal tissues were fixed with 10% neutral buffered formalin (NBF) overnight at 4°C, Swiss rolled, and fixed for 2 more days. Paraffin-embedded sections were cut (4 μm) and immunostaining was performed as previously reported.[17] Tissues were incubated with antibodies listed in Supplemental Table 1. Fluorescence signals were visualized using a Nikon Ti-E microscope with an A1R laser scanning confocal system (Nikon Instruments Inc., Melville, NY). $n = 4$–5 mice per group were analyzed.

Digital Image Analysis

The digital image analysis method for determining apical area was developed at the Digital Histology Shared Resource DHSR core at Vanderbilt University Medical Center. Sections of small intestine were stained with rabbit antibodies against SGLT1 or NHE3, followed by fluorescently-conjugated anti-rabbit IgG antibody and directly conjugated antibodies against villin, ACTG1, and ß-catenin. Nuclei were counterstained with Hoechst 33342 and used for autofocusing. Whole slides were scanned by an Aperio Versa 200 (Leica Biosystems, Buffalo Grove, IL) with a 20x objective, and individual channels were extracted as greyscale images. A probability map of apical surface area was made by pixel classification in Ilastik.[24] Area of apical and total tissue, and immuno-positive area for SGLT1 or NHE3 in apical and in total tissue area, respectively were measured using Cell Profiler™.[25]

Short-circuit current measurements in Üssing chamber system

A pair of mucosal-submucosal preparations were obtained from each mouse jejunum and short-circuit current (I_{sc}) was recorded under voltage-clamp conditions in an Üssing chamber system with a 0.1 cm^2 window area (Physiologic Instruments, San Diego, CA), as previously described.[18] Tissue resistance (R_t) was measured every 5 sec with a bipolar pulse of 3 mV, 200 ms duration. Baseline I_{sc} and R_t were determined after a 30 min stabilization period. Basal CFTR activity was determined as the decrease in I_{sc} (I_{sc}) by (R)-BPO-27 (10 μM) in one preparation. SGLT1 activity in the presence of 11 mM (198 mg/dl) glucose was determined as phlorizin (0.1 mM)-sensitive I_{sc}. Carbachol and forskolin (10 μM each) were applied into the serosal bath to compare Cl⁻ secretory responses in the presence or absence of (R)-BPO-27. CFTR dependency of cAMP-stimulated secretion was assessed by post-

application of (R)-BPO-27 after forskolin administration. To investigate baseline I_{sc} without luminal glucose and to determine electrogenic amino acid transporter functions, glucose was replaced with mannitol in the mucosal bath. A synthetic dipeptide glycilsarcosin (20 mM) and $_L$-glutamate (20 mM) were added into the mucosal bath and peak values of I_{sc} were measured.[26] Dimethylsulfoxide less than 0.3% in the bathing solution did not affect the I_{sc} or R_t.

In vitro induced MYO5B-knockout (iKO) enteroids and immunostaining

Enteroids were generated from jejunal crypts of four adult *VilCre^ERT2;Myo5b^flox/flox* mice that did not receive tamoxifen and grown in IntestiCult™ OGM (06005, StemCell Technologies) as previously reported.[18] Cre recombinase was induced *in vitro* by incubating with 1 μM 4-hydroxy-tamoxifen (SML1666, Sigma) for 24 hours. Control wells were incubated with vehicle (EtOH, 0.8% v/v). The media was replaced with complete minigut media that lacks Wnt3a to enhance enterocyte differentiation as reported,[27, 28] and replaced every day with supplementation of LPA (5 μM) or vehicle for 48 hours. The treated enteroids were fixed in Matrigel with 10% NBF for 30 min at room temperature, rinsed with PBS containing eosin, and embedded in HistoGel™ (HG-4000-012; Thermo Scientific) to make paraffin-embedded sections. In sections immunostained for SGLT1, the percentage of SGLT1-positive cells in each organoid section and the percentage of cells with brush border localization in SGLT1-positive cells were counted under a fluorescence microscope with a 40x objective. Total cell number and brush border were defined by nuclei staining and ACTG1 immunoreactivity, respectively.

Statistical analysis

Statistical differences were determined using GraphPad Prism 8 with a significant *P* value of 0.05. The test used in each analysis is described in the figure legends.

Results

Administration of LPA improved brush border maturation in MYO5B-knockout mice.

We utilized *VilCre^ERT2;Myo5b^flox/flox* mice to model the severe diarrhea induced by MYO5B loss as seen in Microvillus Inclusion Disease (MVID). *In vivo* induction of Cre recombinase in the intestinal epithelia of *VilCre^ERT2;Myo5b^flox/flox* mice significantly decreased body weight compared with tamoxifen-injected control mice at 3 and 4 days after tamoxifen administration. LPA in the present study is 1-oleoyl-LPA (18:1), as per the IUPHAR definition, which is a well-studied, endogenous LPA in both mice and humans. MYO5B deficiency in the intestinal epithelia was confirmed by immunostaining for MYO5B (Supplemental Figure 3). H&E staining and immunohistochemistry for the proliferation marker Ki67 showed that villus blunting in MYO5B-knockout jejunum was prevented by LPA, but expanded crypt length that represents hyperproliferation was not altered (Figure 1A and Supplemental Figure 4). There was no significant difference in smooth muscle thickness between control and MYO5B-knockout tissues (Mean ± SD: control, 29.6 ± 3.09 *vs.* knockout, 29.8 ± 4.00 μm, *P* = 0.92, *n* = 5 mice). Villus epithelial cells in MYO5B-knockout jejunum showed reduced brush border height and density in frozen sections and TEM images (Figures 1A, 1B, Supplemental Figure 5). Administration

of LPA, particularly by intraperitoneal (ip) injection, restored microvillus structure, but did not prevent microvillus inclusion formation. TEM images revealed that LPA significantly decreased the size of large multivesicular body-like vacuoles in MYO5B-knockout enterocytes (Supplemental Figure 5). However, daily administration of LPA by either oral gavage (og) or ip injection did not significantly change the body weight loss after induced MYO5B loss (Figure 1C). *Myo5b*[flox/flox] and *VilCre*[ERT2]; *Myo5b*[fox/−] mice demonstrated normal phenotypes after tamoxifen administration. Both genotypes were used as controls with tamoxifen administration in physiological experiments and immunostaining to account for any influence of tamoxifen.

LPA suppressed endogenous hyperactivity of CFTR and increased activity of SGLT1 in MYO5B-knockout mouse jejunum.

The functions of apical CFTR, SGLT1, and amino acid transporters in treated mouse jejunum were evaluated in Üssing chambers. Total mucosal resistance showed no difference between control and MYO5B-knockout tissues, with or without luminal glucose (Supplemental Figure 6A and 6C). FITC-dextran (4 kD) permeability was not significantly altered by MYO5B loss, compared with control tissues (Supplemental Figure 6D). These results suggest that MYO5B-knockout mucosa possesses comparable paracellular permeability. The contributions of CFTR and SGLT1 to the baseline short-circuit current (I_{sc}) in steady-state were assessed using inhibitors. Compared to control jejunum, total I_{sc} was significantly lower in MYO5B-knockout, consistent with decreased SGLT1- and other transporter-mediated currents (Figure 2A). In the absence of luminal glucose, we observed no significant difference in baseline I_{sc} between control and MYO5B-knockout jejunum, supporting the presence of absorptive current in the steady state (Supplemental Figure 6C). Basal CFTR-dependent current was significantly decreased in MYO5B-knockout mice treated by ip LPA or the synthetic LPA receptor 2 (LPAR2) agonist, GRI977143 (Figure 2B). SGLT1 activities were increased in the jejunum of mice who received og or ip administration of LPA, independent of LPAR2 signaling (Figure 2C).

CFTR mediates the majority of anion secretion in response to intracellular Ca^{2+} and cAMP elevation.[29] To assess CFTR function in stimulated conditions, an acetylcholine analogue, carbachol, and the adenylate cyclase activator, forskolin were applied in the presence or absence of a maximal dose of R-BPO-27.[30, 31] Stimulated I_{sc} was similar in control and MYO5B-knockout jejunum, and R-BPO-27 significantly decreased the response to both carbachol and forskolin (Supplemental Figure 7). The CFTR-dependent portion of stimulated secretion was significantly increased in MYO5B-knockout jejunum in forskolin-evoked, but not carbachol-evoked response, indicating that cAMP-activated maximal CFTR activity may be upregulated by MYO5B deficiency (Figures 2D and 2E). CFTR dependence in the activated secretory state was further evaluated by adding R-BPO-27 after the peak of forskolin stimulation (Figure 2F). The stimulated I_{sc} in control tissues was reduced 80% by post-application of R-BPO-27, suggesting that the remaining 20% of I_{sc} was dependent on other Cl^- channels, such as ANO1 expressed in the villus apical membrane.[32] In MYO5B-knockout jejunum from mice with vehicle or og LPA administration, R-BPO-27 decreased I_{sc} more than the values of forskolin-evoked I_{sc} increase, consistent with the abnormal basal CFTR activity. Administration of ip LPA or GRI977143 suppressed basal CFTR activity, but

cAMP-activated I_{sc} was completely reversed by R-BPO-27, indicating that LPAR2 activation did not alter CFTR expression (Figure 2E and 2F). Other electrogenic nutrient transporters for glutamic acid and dipeptide were investigated under luminal glucose-free conditions to maximize amino acid absorption.[26, 33] Glutamate- and a dipeptide (glycilsarcosine)-induced I_{sc} increases were significantly lower in MYO5B-knockout than Control, and did not significantly recover following by LPA injection (Figure 2G and 2H).

MYO5B deletion had a broad impact on gene expression patterns in jejunal epithelial cells.

To evaluate the global changes in gene expression following MYO5B loss, we performed RNA sequencing (RNA-seq) on jejunal epithelial cells from tamoxifen-induced *VilCre^ERT2;Myo5b^flox/flox* (knockout) mice that received LPA or vehicle for 4 days, and from uninduced *VilCre^ERT2;Myo5b^flox/flox* mice (Control) to keep identical genetic backgrounds. RNA-seq revealed that 844 genes were significantly down-regulated, and 657 genes were up-regulated by tamoxifen-induced MYO5B loss compared to Control (Supplemental Figure 8A). LPA administration had little effect on gene expression patterns, suggesting that the beneficial effects of LPA were more likely through post-transcriptional regulation (Supplemental Figure 8B). Only 5 genes, *Cd79a, Ppp1r16b, Adamdec1, Lyz2*, and *Hmgcs2*, were both significantly downregulated by MYO5B deletion and upregulated by LPA administration (Supplemental Figure 8C). While *Hmgcs2* encodes a rate-limited ketogenic enzyme, which is involved in epithelial differentiation,[34] the functions of the other four genes are unknown in epithelial cells. GO enrichment analysis (Gene Ontology Consortium)[35] demonstrated altered expression patterns of genes that are involved in transmembrane transporter activity and lysosomes associated with MYO5B loss (Supplemental Figure 9). Among proteinases, *ctse* (cathepsin E) was upregulated over 12-fold. MYO5B loss increased expression of several genes, including Myo5c and Myo1c. The expression of numerous nutrient transporters was decreased in MYO5B-knockout enterocytes, including those for glucose, vitamins, metals, and amino acids, while the expression of mRNA for *slc5a1* (SGLT1) was increased by LPA, but not significantly (Supplemental Figure 9). The transcription of other brush border proteins that were investigated in our previous study,[18] such as *slc9a3* (NHE3), *cftr,* aquaporins, *dpp4, api* (alkaline phosphatase), or sis (sucrase isomaltase) was not altered, suggesting that MYO5B loss influences the trafficking of these membrane proteins, but not their transcription. KEGG pathway analysis (Kyoto Encyclopedia of Genes and Genomes; http://www.genome.jp/kegg/) showed that the majority of down-regulated genes were involved in metabolic pathways, and that up-regulated genes were involved in ribosome biogenesis and cell division (Supplemental Figure 10). Several transcription factors specific for intestinal cell types were identified previously in a single-cell RNA-seq study.[8] In the present RNA-seq data, we found that three stem cell transcription factors *(Tgif1, Macom and Arid5b)* were significantly increased in tamoxifen-induced MYO5B-knockout jejunum, whereas two tuft cell-specific transcription factors *(Spib and Pou2f3)* were significantly decreased (Supplemental Figure 11). These results indicate that MYO5B loss disrupts the maturation and differentiation of epithelial cells.

LPA partially normalized the brush border localization of SGLT1 and NHE3 and the over-expression of cathepsins D and E and Rab7 in MYO5B-knockout mouse jejunum.

In our previous studies, larger than normal lysosome associated membrane protein (LAMP) 1-positive lysosomes were observed in MYO5B-knockout mice.[18] Due to the prominent changes in the expression of lysosomal-related genes observed in RNA-seq (Supplemental Figure 9), we next examined lysosomal elements in MYO5B-knockout mice in more detail. Expression of the lysosomal protease cathepsin D was found in cytosolic vesicles in enterocytes in MYO5B-knockout mice, but not in control tissues or the regions of LPA-given mouse intestines that expressed SGLT1 on the brush border (Figure 3). SGLT1 immunoreactivity was diffuse within the cytoplasm of MYO5B-knockout epithelia and was not detected in either gamma-actin (ACTG1)-positive inclusions or large LAMP1-positive lysosomes (Supplemental Figure 12). Daily administration of LPA, but not GRI977143, increased brush border localization of SGLT1 in regions of villi (Figure 3 and 6). Glutamic acid is absorbed through several transporters, including EAAT3 (also known as SLC1A1),[36] but the exact functional transporter has not been identified with knockout animals. Dipeptide absorption is likely mediated by PEPT1 (known as Slc15a1),[26] which was identified on the villus brush border in control tissues (Supplemental Figure 13). The apical PEPT1 signals were diffuse in MYO5B-knockout tissues similarly to what observed for SGLT1 and NHE3. In LPA-injected Myo5B-knockout mice, some villus cells had PEPT1 immunostaining on the brush border (Supplemental Figure 13). In contrast, predominant expression of CFTR was identified in crypts and lower villus regions in control jejunum, and its expression was maintained on the apical membranes of enterocytes in MYO5B-knockout tissues (Figure 3, Supplemental Figure 13), indicating that CFTR does not traffic through a MYO5B-dependent mechanism.

Epithelial expression of Rab7, which regulates the trafficking through late-endosomes and formation of autophagic vacuoles,[37, 38] was detected in MYO5B-knockout tissues and frequently included in large LAMP1-positive vacuoles (Figure 4). Sub-apical localization of NHE3 and Rab7 in MYO5B-knockout epithelial cells were partially normalized by administration of either og- or ip LPA (Figure 4). Consistent with an increase in gene expression, the immunostaining for cathepsin E was frequently found in large LAMP2-positive vacuoles in MYO5B-knockout tissues, but was only weakly detected on apical membranes in control tissues (Figure 5). ACTG1 was strongly expressed in the brush border microvilli in control tissues, whereas MYO5B deficiency resulted in a thin apical ACTG1 staining, similar in intensity to the basolateral membrane. Intraperitoneal LPA administration partially improved brush border ACTG1 staining in parallel with the suppression of cathepsin E expression and a reduction in large lysosomal vacuoles (Figure 5, Supplemental Figure 14). LAMP1/2-positive large vacuoles in MYO5B-knockout epithelial cells co-stained for both cathepsins D and E, which were not detected in the cytoplasm of control tissues (Supplemental Figure 14). These observations indicate that MYO5B loss upregulated protein degradation in villus cells consistent with large multivesicular bodies, which were identified in TEM sections (Supplemental Figure 5), and LPA injection appeared to reduce these changes.

We sought to quantify the apical surface area and brush border localization of NHE3 and SGLT1 in whole immunostained sections by digital image analysis. Apical surface area was defined as whole cell membrane (ACTG1) plus brush border (villin) minus basolateral membrane (ß-catenin) (Supplemental Figure 15). Apical area was outlined both in control and MYO5B-knockout tissues, independent from diffuse villin staining (Figure 6A). MYO5B-knockout jejunum showed approximately half the apical surface area as compared to controls, and LPA administration significantly increased apical area (Figure 6B). The brush border localization of SGLT1 and NHE3 was significantly reduced by 60% and 73%, respectively, in MYO5B-knockout tissues (Figure 6C and 6D). MYO5B-knockout mice receiving either ip or og LPA demonstrated a significant improvement in SGLT1 localization (Figure 6C). Effects of LPA administration on NHE3 localization were varied and only ip-LPA significantly increased apical NHE3 (Figure 6D). Immunoreactivity for internalized NHE3 was strong and occupied large areas in MYO5B-knockout tissues (Figure 6A). The apical NHE3 ratio in some og LPA-given tissues may be confounded by the significantly taller villi compared to vehicle-treated MYO5B-knockout tissues (Supplemental Figure 4). No significant improvement was detected in the GRI977143-treated group, indicating that the mechanism of LPA-induced brush border re-establishment is likely LPAR2 independent.

LPA had no effect on altered expression of claudin-2 and claudin-15

Claudin-2 and claudin-15 regulate paracellular sodium recycling, which is essential for sodium-dependent nutrient absorption.[39] RNA-seq data revealed that claudin-2 expression was upregulated by MYO5B deletion and claudin-15 was downregulated in jejunal epithelial cells (Supplemental Figure 9). Occludin and other predominant claudins, such as claudin-4, claudin-7, and claudin-12 were not altered. Control jejunum showed immunostaining for claudin-2 limited to tight junctions in the crypts. MYO5B-knockout mice received vehicle or LPA showed intracellular expression of claudin-2 in enterocytes, in addition to tight junctions in the extended crypt area (Supplemental Figure 16). Claudin-15 was expressed on tight junctions of villus and crypt cells in control enterocytes. In contrast, diffuse expression of claudin-15 in cytoplasm was found in MYO5B-knockout intestine and administration of LPA did not restore the localization of claudin-15 at junctions (Supplemental Figure 17).

LPA improved brush border maturation and transporter trafficking in vitro

To investigate whether LPA has cell-autonomous effects on brush border maturation and transporter trafficking, enteroids were generated from *VilCre^{ERT2};Myo5b^{flox/flox}* mouse jejunum and cultured with LPA in differentiation media. SGLT1, NHE3, and DPP IV were localized on the brush border membrane in control enteroids without Cre-activation (Figure 7, Supplemental Figures 18 and 19). Control and LPA-supplemented *in vitro*-induced MYO5B-knockout (iKO) organoids demonstrated approximately 60% SGLT1-positive cells, indicating mature absorptive cells. Vehicle-treated iKO enteroids showed significantly fewer (average 25%) SGLT1-expresing cells (Figure 7B). More than 80% of cells did not express SGLT1 on the apical membrane in iKO enteroids, whereas LPA supplementation significantly improved SGLT1 localization (Figure 7C). The iKO enteroids incubated with hydroxytamoxifen showed immature microvilli, as demonstrated by ACTG1 staining, compared to control enteroids (Supplemental Figure 18). In addition, the iKO enteroids showed significantly less apical SGLT1-immunoreactivity and internalized NHE3 and DPP

IV in the cytoplasm, similar to MYO5B-knockout jejunal tissues (Figure 7C, Supplemental Figures 18 and 19). Supplementation of LPA into the enteroid medium caused iKO enteroids to develop brush border microvilli and partially re-established the localization of SGLT1, NHE3, and DPP IV, indicating that LPA directly stimulates brush border maturation in MYO5B deficient enterocytes (Figure 7, Supplemental Figures 18 and 19).

Discussion

We previously proposed that a critical mechanism of diarrheal pathology caused by MYO5B loss is the sustained Cl$^-$ secretion via CFTR and the deficits of apical Na$^+$ absorption through SGLT1 and NHE3.[18] In this study, we have investigated the potential therapeutic effects of LPA, which possesses broad bioactivities on the maturation and transporter functions of epithelial cells, in an intestine-specific induced MYO5B-knockout mouse model. Our results demonstrate that LPA can induce a partial return of critical sodium transporters to the apical membrane. These findings suggest that the blockade in apical trafficking can be bypassed as a potential therapeutic intervention in MVID.

Activation of LPA receptor LPAR2 inhibits CFTR-dependent anion/water secretion via Na$^+$/H$^+$ exchanger regulatory factor (NHERF)2.[9, 40] Luminal perfusion of LPA or the recently developed LPAR2 agonist, Rx100, suppresses CFTR-dependent water secretion stimulated by cholera toxin in mouse ileum, but not in LPAR2-knockout mice.[10, 41] Direct binding of LPAR2 to NHERF2 attenuates CFTR activity via a G$_i$-mediated pathway in the epithelial cell line HT29-CL19A,[10] but not in NHERF2-knockout mice.[40] Consistent with these reports, Üssing chamber assays in this study demonstrated that LPA and a commercially available LPAR2 agonist, GRI977143, significantly suppressed basal CFTR activity, which is abnormally upregulated in MYO5B-knockout jejunum (Figure 2). Since *Cftr* gene expression and CFTR immunostaining were not altered by MYO5B loss or LPA administration, CFTR function is likely regulated by LPA-sensitive trafficking mechanisms. GRI977143 had little effect on glucose absorption or transporter localization (Figures 2, 3, 4, and 6). Although LPAR2 agonists have mucosal protective effects, such as preventing apoptosis and enhancing stem cell survival and cell migration,[6] other targets are needed to enhance nutrient absorption and to treat MVID symptoms in addition to LPAR2 activation.

LPA enhances fluid absorption and NHE3 trafficking from the terminal web to the microvilli dependent on LPAR5 and NHERF2, but independent from LPAR2 in healthy and cholera toxin-stimulated mice.[7, 11] When epithelial cells are activated by cAMP or Ca^{2+} signaling, endocytosis of NHE3 from the apical membrane and membrane recruitment of CFTR are likely processed simultaneously,[42] suggesting that NHERF2 may play a role as a switch of villus epithelial function between absorption and secretion. Immunostaining and digital image analysis presented in this study indicate that MYO5B deficiency causes the mislocalization of NHE3 away from apical membrane, and that LPA administration partially re-established the brush border localization of NHE3 (Figures 3 and 6). Incubation of iKO enteroids with LPA showed more uniform expression of NHE3 compared to jejunal tissues that showed patchy re-expression of NHE3 in the brush border along villi (Supplemental Figure 19). Since enterocytes develop their mature brush border characteristics as they emerge from the crypts, we speculate that exposure to adequate concentrations of LPA are

required during this cell maturation period to establish the brush border and apical transporters such as NHE3. The once daily LPA administration regimen used in these mouse studies may not be sufficient to impact all epithelial cells *in vivo.*

Co-transport of water with Na^+ and glucose accounts for approximately 50% of the total water absorption in human intestine dependent on SGLT1.[20] Despite the importance of its function, the trafficking and regulatory mechanisms affecting SGLT1 are mostly unknown. The present study demonstrated that the immunoreactivity of apical SGLT1 was reduced in MYO5B-knockout enterocytes, consistent with gene expression (Figures 6, 7, Supplemental Figure 9). Since SGLT1 is expressed only in highly differentiated enterocytes, which do not utilize glucose as essential energy source,[43] SGLT1 expression is likely correlated with enterocyte maturation. A specific antibody against mouse SGLT1 and two antibodies against individual epitopes of mouse CFTR demonstrated distinct expression patterns for these transporters (Figure 3, Supplemental Figure 13). CFTR was predominantly found on the apical membrane in cells of crypts and lower villi similarly in control and MYO5B-knockout tissues. Although villus CFTR immunoreactivity has been reported in the duodenum, a CFTR inhibitor works only from the serosal side and the actual functional site of CFTR cannot be distinguished.[18] Consistently, intraperitoneally-delivered LPA or GRI977143, but not gavaged LPA, inhibited basal CFTR activities (Figure 2). Furthermore, MYO5B loss-induced microvillus inclusions were identified in villus cells, but not in crypts.[17, 18] These observations suggest that the predominant site for CFTR function may reside in crypt cells and that CFTR trafficking does not primarily utilize a Myo5b-dependent trafficking mechanism.

In Üssing chamber assays, SGLT1-dependent current was increased by og and ip LPA by 80% and 130%, respectively, supporting the LPA-induced functional expression of SGLT1 on the brush border (Figures 2 and 6). Re-establishment of microvillus height and SGLT1 localization was patchy in LPA-given mouse intestines (Figure 1 and 3). LPA-supplemented MYO5B iKO enteroids showed a more uniform expression pattern (Figure 7), suggesting that continuous exposure to LPA in early stages of differentiation may be an effective strategy to improve brush border maturation and proper SGLT1 expression. Brush border localization of the proton-coupled peptide transporter 1 (PEPT1) and I_{sc} change in response to luminal challenge of glycylsarcosine were reduced by MYO5B loss and not significantly improved by ip LPA (Supplemental Figures 4 and 13). Taking these results together, different types of transporters in different stages of cell maturation may be regulated by distinct trafficking mechanisms.

The present RNA-seq analysis showed that MYO5B loss significantly alters the gene expression patterns for proteins associated with lysosomal function (Supplemental Figure 9). Our immunohistochemical studies showed a remarkable increase in cytoplasmic accumulation of cathepsins D and E, and Rab7 following MYO5B deletion (Figure 3, 4, and 5). Rab7-dependent trafficking is required to form multivesicular bodies and transfer to lysosomes for degrading membrane receptors and transporters.[37, 44] All of these molecules were frequently identified inside of LAMP1/2-positive multivesicular bodies, which were also observed in TEM sections in MYO5B-knockout tissues, suggesting that protein degradation is upregulated in MYO5B-knockout enterocytes together with the mis-

trafficking of apical transporters. It is unclear whether a "traffic jam" of membrane transporters accumulating in the cytoplasm induces an abnormal autophagic pathway or if upregulated Rab7 causes transporter loss. Regardless, the patchy improvement of epithelial cells in LPA-given MYO5B-knockout tissues indicates that the brush border maturation and proper localization of NHE3 and SGLT1 are associated with the suppression of abnormal lysosomal activities independent of the formation of microvillus inclusions.

Claudin-2 and claudin-15 form paracellular gates for monovalent cations in the small intestine and their expression increases Na^+ permeability. Adult claudin-15-knockout mice show low Na^+ conductance and reduced SGLT1-dependent glucose absorption, suggesting that the Na^+ recycling from submucosa to the lumen is essential for the activities of sodium-dependent nutrient transporters.[45] In our current observations, MYO5B-knockout mice showed an increase in claudin-2 in parallel with an increase in crypt height, and a decrease in claudin-15 transcription and immunostaining in villus and crypt cells (Supplemental Figures 4, 16, and 17). Total tissue resistance and dextran permeability, as determined in Üssing chambers, were comparable to that of control mice (Figure 2, Supplemental Figure 6). This imbalance of claudin expression is likely not detectable by measuring total permeability. Unfortunately, administration of LPA did not normalize the expression pattern of these claudins or alter hyperproliferation of crypt cells in MYO5B-knockout mice. The present RNA-seq results demonstrated significant changes induced by MYO5B deletion in cell type-specific transcription factors with an increase in stem cell markers. Furthermore, MYO5B loss downregulated a ketogenic enzyme *Hmgcs2,* which contributes to proper differentiation,[34] suggesting that MYO5B serves an important role in proliferating cells for epithelial differentiation (Supplemental Figures 8 and 11). Further therapeutic efforts targeting cell differentiation and junctional sodium conductance may be needed to treat malabsorption in MYO5B-knockout mice, in addition to the enhanced brush border maturation by LPA administration. In the CaCo-2 cell line, a supra-physiological dose (100 μM) of LPA or an LPAR2 agonist, dodecylphosphate increases Cl^- absorption via membrane trafficking of the downregulated in adenoma (DRA; as known as Slc26a3).[46] The present study did not investigate DRA because of its low expression level in mouse jejunum. Since DRA is an important target for anti-diarrheal strategies in the human intestine,[47] the effect of LPA has to be clarified in human enteroids in future studies. In humans, food-derived phosphatidic acids are converted to LPA by secreted PLA_2 ($sPLA_2$) within the gastrointestinal lumen, a mechanism which is likely absent in C57BL/6 mice. Oral LPA, as well as phosphatidylcholine and phosphatidic acid, reduces aspirin-induced gastric ulcers in ICR mice that express $sPLA_2$ in the gastric lumen.[48] In the present study, orally gavaged LPA prevented villus blunting in MYO5B-knockout mice more than intraperitoneal LPA administration. Intraperitoneally delivered LPA further normalized abnormal CFTR and SGLT1 functions, as well as microvillus height and transporter localization. Although the absorptive mechanism and dynamics of LPA has not yet been identified, those observations suggest that long-acting LPA analogues or LPA precursors, such as phosphatidic acid, in oral rehydration solution may be a promising treatment for MVID patients.

In summary, our present study demonstrates that daily administration of MYO5B-knockout mice with LPA improves SGLT1 function, NHE3 localization, villus blunting, and brush border maturation, along with reducing abnormal CFTR activity and cathepsin expression in

the multivesicular bodies. On the other hand, LPA does not alter hyperproliferation, microvillus inclusion formation, or abnormal claudin-2 and claudin-15 localization that are induced by MYO5B deficiency. Loss of MYO5B leads to a variety of epithelial deficits through multiple pathways, resulting in malabsorption with secretory diarrhea. Our findings suggest that intestinal epithelial defects in MVID patients may be ameliorated with orally active ligands. Thus, intestinal epithelial cells can mobilize intracellular trafficking pathways that can bypass an apical trafficking blockade and can re-establish elements of apical brush border differentiation. Actual LPA target cells and therapeutic pathways should be identified in future studies.

Supplementary Material

Refer to Web version on PubMed Central for supplementary material.

Acknowledgements

Abbreviations:

ACTG1	gamma-actin
CFTR	cystic fibrosis transmembrane conductance regulator
CTS	cathepsin
DPP IV	dipeptidyl-peptidase IV
ip	intraperitoneal
I_{sc}	short-circuit current
LAMP	lysosomal-associated membrane protein
LPA	lysophosphatidic acid
Myo5b	myosin Vb
MVID	microvillus inclusion disease
NHE3	sodium/proton exchanger 3
PEPT1	peptide transporter 1

pERM	phosphorylated ezrin/radixin/moesin
PL	phospholipases
og	oral gavage
R_t	tissue resistance
SGLT1	sodium-dependent glucose transporter 1
TEM	transmission electron microscopy

References

1. Lee BH, Choi SH, Kim HJ, et al. Plant Lysophosphatidic Acids: A Rich Source for Bioactive Lysophosphatidic Acids and Their Pharmacological Applications. Biol Pharm Bull 2016;39:156–62. [PubMed: 26830477]

2. Baker DL, Desiderio DM, Miller DD, et al. Direct quantitative analysis of lysophosphatidic acid molecular species by stable isotope dilution electrospray ionization liquid chromatography-mass spectrometry. Anal Biochem 2001;292:287–95. [PubMed: 11355863]

3. Aoki J Mechanisms of lysophosphatidic acid production. Semin Cell Dev Biol 2004;15:477–89. [PubMed: 15271293]

4. Konno T, Kotani T, Setiawan J, et al. Role of lysophosphatidic acid in proliferation and differentiation of intestinal epithelial cells. PLoS One 2019;14:e0215255. [PubMed: 31017922]

5. Aikawa S, Hashimoto T, Kano K, et al. Lysophosphatidic acid as a lipid mediator with multiple biological actions. J Biochem 2015;157:81–9. [PubMed: 25500504]

6. Tigyi GJ, Johnson LR, Lee SC, et al. Lysophosphatidic acid type 2 receptor agonists in targeted drug development offer broad therapeutic potential. J Lipid Res 2019;60:464–474. [PubMed: 30692142]

7. Lin S, Yeruva S, He P, et al. Lysophosphatidic acid stimulates the intestinal brush border Na(+)/H(+) exchanger 3 and fluid absorption via LPA(5) and NHERF2. Gastroenterology 2010;138:649–58. [PubMed: 19800338]

8. Haber AL, Biton M, Rogel N, et al. A single-cell survey of the small intestinal epithelium. Nature 2017;551:333–339. [PubMed: 29144463]

9. Choi JW, Herr DR, Noguchi K, et al. LPA receptors: subtypes and biological actions. Annu Rev Pharmacol Toxicol 2010;50:157–86. [PubMed: 20055701]

10. Li C, Dandridge KS, Di A, et al. Lysophosphatidic acid inhibits cholera toxin-induced secretory diarrhea through CFTR-dependent protein interactions. J Exp Med 2005;202:975–86. [PubMed: 16203867]

11. Jenkin KA, He P, Yun CC. Expression of lysophosphatidic acid receptor 5 is necessary for the regulation of intestinal Na(+)/H(+) exchanger 3 by lysophosphatidic acid in vivo. Am J Physiol Gastrointest Liver Physiol 2018;315:G433–g442. [PubMed: 29792531]

12. Muller T, Hess MW, Schiefermeier N, et al. MYO5B mutations cause microvillus inclusion disease and disrupt epithelial cell polarity. Nat Genet 2008;40:1163–5. [PubMed: 18724368]

13. Erickson RP, Larson-Thome K, Valenzuela RK, et al. Navajo microvillous inclusion disease is due to a mutation in MYO5B. Am J Med Genet A 2008;146a:3117–9. [PubMed: 19006234]

14. Vogel GF, Janecke AR, Krainer IM, et al. Abnormal Rab11-Rab8-vesicles cluster in enterocytes of patients with microvillus inclusion disease. Traffic 2017;18:453–464. [PubMed: 28407399]

15. Thiagarajah JR, Kamin DS, Acra S, et al. Advances in Evaluation of Chronic Diarrhea in Infants. Gastroenterology 2018;154:2045–2059.e6. [PubMed: 29654747]

16. Schneeberger K, Vogel GF, Teunissen H, et al. An inducible mouse model for microvillus inclusion disease reveals a role for myosin Vb in apical and basolateral trafficking. Proc Natl Acad Sci U S A 2015;112:12408–13. [PubMed: 26392529]

17. Weis VG, Knowles BC, Choi E, et al. Loss of MYO5B in mice recapitulates Microvillus Inclusion Disease and reveals an apical trafficking pathway distinct to neonatal duodenum. Cell Mol Gastroenterol Hepatol 2016;2:131–157. [PubMed: 27019864]

18. Engevik AC, Kaji I, Engevik MA, et al. Loss of MYO5B Leads to Reductions in Na(+) Absorption With Maintenance of CFTR-Dependent Cl(−) Secretion in Enterocytes. Gastroenterology 2018;155:1883–1897.e10. [PubMed: 30144427]

19. Martin MG, Turk E, Lostao MP, et al. Defects in Na+/glucose cotransporter (SGLT1) trafficking and function cause glucose-galactose malabsorption. Nat Genet 1996;12:216–20. [PubMed: 8563765]

20. Loo DD, Wright EM, Zeuthen T. Water pumps. J Physiol 2002;542:53–60. [PubMed: 12096049]

21. Kaji I, Akiba Y, Konno K, et al. Neural FFA3 activation inversely regulates anion secretion evoked by nicotinic ACh receptor activation in rat proximal colon. J Physiol 2016;594:3339–52. [PubMed: 26854275]

22. Gorboulev V, Schurmann A, Vallon V, et al. Na(+)-D-glucose cotransporter SGLT1 is pivotal for intestinal glucose absorption and glucose-dependent incretin secretion. Diabetes 2012;61:187–96. [PubMed: 22124465]

23. McHugh DR, Steele MS, Valerio DM, et al. A G542X cystic fibrosis mouse model for examining nonsense mutation directed therapies. PLoS One 2018;13:e0199573. [PubMed: 29924856]

24. Berg S, Kutra D, Kroeger T, et al. ilastik: interactive machine learning for (bio)image analysis. Nat Methods 2019;16:1226–1232. [PubMed: 31570887]

25. Jones TR, Kang IH, Wheeler DB, et al. CellProfiler Analyst: data exploration and analysis software for complex image-based screens. BMC Bioinformatics 2008;9:482. [PubMed: 19014601]

26. Chen M, Singh A, Xiao F, et al. Gene ablation for PEPT1 in mice abolishes the effects of dipeptides on small intestinal fluid absorption, short-circuit current, and intracellular pH. American journal of physiology. Gastrointestinal and liver physiology 2010;299:G265–G274. [PubMed: 20430876]

27. Mahe MM, Aihara E, Schumacher MA, et al. Establishment of Gastrointestinal Epithelial Organoids. Curr Protoc Mouse Biol 2013;3:217–40. [PubMed: 25105065]

28. Merenda A, Fenderico N, Maurice MM. Wnt Signaling in 3D: Recent Advances in the Applications of Intestinal Organoids. Trends Cell Biol 2020;30:60–73. [PubMed: 31718893]

29. Seidler U, Blumenstein I, Kretz A, et al. A functional CFTR protein is required for mouse intestinal cAMP-, cGMP- and Ca(2+)-dependent HCO3-secretion. The Journal of physiology 1997;505 (Pt 2):411–423. [PubMed: 9423183]

30. Kim Y, Anderson MO, Park J, et al. Benzopyrimido-pyrrolo-oxazine-dione (R)-BPO-27 Inhibits CFTR Chloride Channel Gating by Competition with ATP. Molecular pharmacology 2015;88:689–696. [PubMed: 26174774]

31. Cil O, Phuan P-W, Gillespie AM, et al. Benzopyrimido-pyrrolo-oxazine-dione CFTR inhibitor (R)-BPO-27 for antisecretory therapy of diarrheas caused by bacterial enterotoxins. FASEB journal : official publication of the Federation of American Societies for Experimental Biology 2017;31:751–760. [PubMed: 27871064]

32. Lee B, Hong G-S, Lee SH, et al. Anoctamin 1/TMEM16A controls intestinal Cl(−) secretion induced by carbachol and cholera toxin. Experimental & molecular medicine 2019;51:91–91.

33. Mace OJ, Lister N, Morgan E, et al. An energy supply network of nutrient absorption coordinated by calcium and T1R taste receptors in rat small intestine. The Journal of physiology 2009;587:195–210. [PubMed: 19001049]

34. Cheng CW, Biton M, Haber AL, et al. Ketone Body Signaling Mediates Intestinal Stem Cell Homeostasis and Adaptation to Diet. Cell 2019; 178:1115–1131.e15. [PubMed: 31442404]

35. Mi H, Muruganujan A, Ebert D, et al. PANTHER version 14: more genomes, a new PANTHER GO-slim and improvements in enrichment analysis tools. Nucleic Acids Res 2019;47:D419–d426. [PubMed: 30407594]

36. Iwanaga T, Goto M, Watanabe M. Cellular distribution of glutamate transporters in the gastrointestinal tract of mice: an immunohistochemical and in situ hybridization approach. Biomedical research (Tokyo, Japan) 2005;26:271–278.

37. Vanlandingham PA, Ceresa BP. Rab7 regulates late endocytic trafficking downstream of multivesicular body biogenesis and cargo sequestration. J Biol Chem 2009;284:12110–24. [PubMed: 19265192]

38. Jager S, Bucci C, Tanida I, et al. Role for Rab7 in maturation of late autophagic vacuoles. J Cell Sci 2004;117:4837–48. [PubMed: 15340014]

39. Wada M, Tamura A, Takahashi N, et al. Loss of claudins 2 and 15 from mice causes defects in paracellular Na+ flow and nutrient transport in gut and leads to death from malnutrition. Gastroenterology 2013;144:369–80. [PubMed: 23089202]

40. Singh AK, Riederer B, Krabbenhoft A, et al. Differential roles of NHERF1, NHERF2, and PDZK1 in regulating CFTR-mediated intestinal anion secretion in mice. J Clin Invest 2009;119:540–50. [PubMed: 19221439]

41. Thompson KE, Ray RM, Alli S, et al. Prevention and treatment of secretory diarrhea by the lysophosphatidic acid analog Rx100. Exp Biol Med (Maywood) 2018;243:1056–1065. [PubMed: 30253666]

42. Jakab RL, Collaco AM, Ameen NA. Physiological relevance of cell-specific distribution patterns of CFTR, NKCC1, NBCe1, and NHE3 along the crypt-villus axis in the intestine. Am J Physiol Gastrointest Liver Physiol 2011;300:G82–98. [PubMed: 21030607]

43. Alpers DH. Is glutamine a unique fuel for small intestinal cells? Curr Opin Gastroenterol 2000;16:155. [PubMed: 17024034]

44. Hurley JH, Emr SD. The ESCRT complexes: structure and mechanism of a membrane-trafficking network. Annu Rev Biophys Biomol Struct 2006;35:277–98. [PubMed: 16689637]

45. Tamura A, Hayashi H, Imasato M, et al. Loss of claudin-15, but not claudin-2, causes Na+ deficiency and glucose malabsorption in mouse small intestine. Gastroenterology 2011;140:913–23. [PubMed: 20727355]

46. Singla A, Dwivedi A, Saksena S, et al. Mechanisms of lysophosphatidic acid (LPA) mediated stimulation of intestinal apical Cl-/OH-exchange. Am J Physiol Gastrointest Liver Physiol 2010;298:G182–9. [PubMed: 19910524]

47. Singh V, Yang J, Chen TE, et al. Translating molecular physiology of intestinal transport into pharmacologic treatment of diarrhea: stimulation of Na+ absorption. Clin Gastroenterol Hepatol 2014;12:27–31. [PubMed: 24184676]

48. Tanaka T, Morito K, Kinoshita M, et al. Orally administered phosphatidic acids and lysophosphatidic acids ameliorate aspirin-induced stomach mucosal injury in mice. Dig Dis Sci 2013;58:950–8. [PubMed: 23161268]

What You Need to Know

Background and context:

Myosin VB (MYO5B) is a trafficking protein required for membrane recycling in gastrointestinal epithelial cells; inactivating mutations cause the congenital diarrheal disease microvillus inclusion disease. MYO5B deficiency in mice causes mislocalization of proteins in intestinal epithelial cells, resulting in malabsorption and secretory diarrhea. Activation of lysophosphatidic acid (LPA) receptors can reduce diarrhea, but requires more study in mouse models of disease.

New findings:

LPA reduced villus blunting and increased sodium/glucose cotransporter activity in intestinal tissues from MYO5B-knockout mice. LPA might therefore regulate a MYO5B-independent trafficking mechanism and brush border maturation.

Limitations:

This study was performed in mice; additional studies are needed in humans.

Impact:

LPA analogues might be developed for treatment of MVID.

Lay Summary:

This study identified a drug that increases intestinal epithelial cell functions in mice that are a model of microvillus inclusion disease.
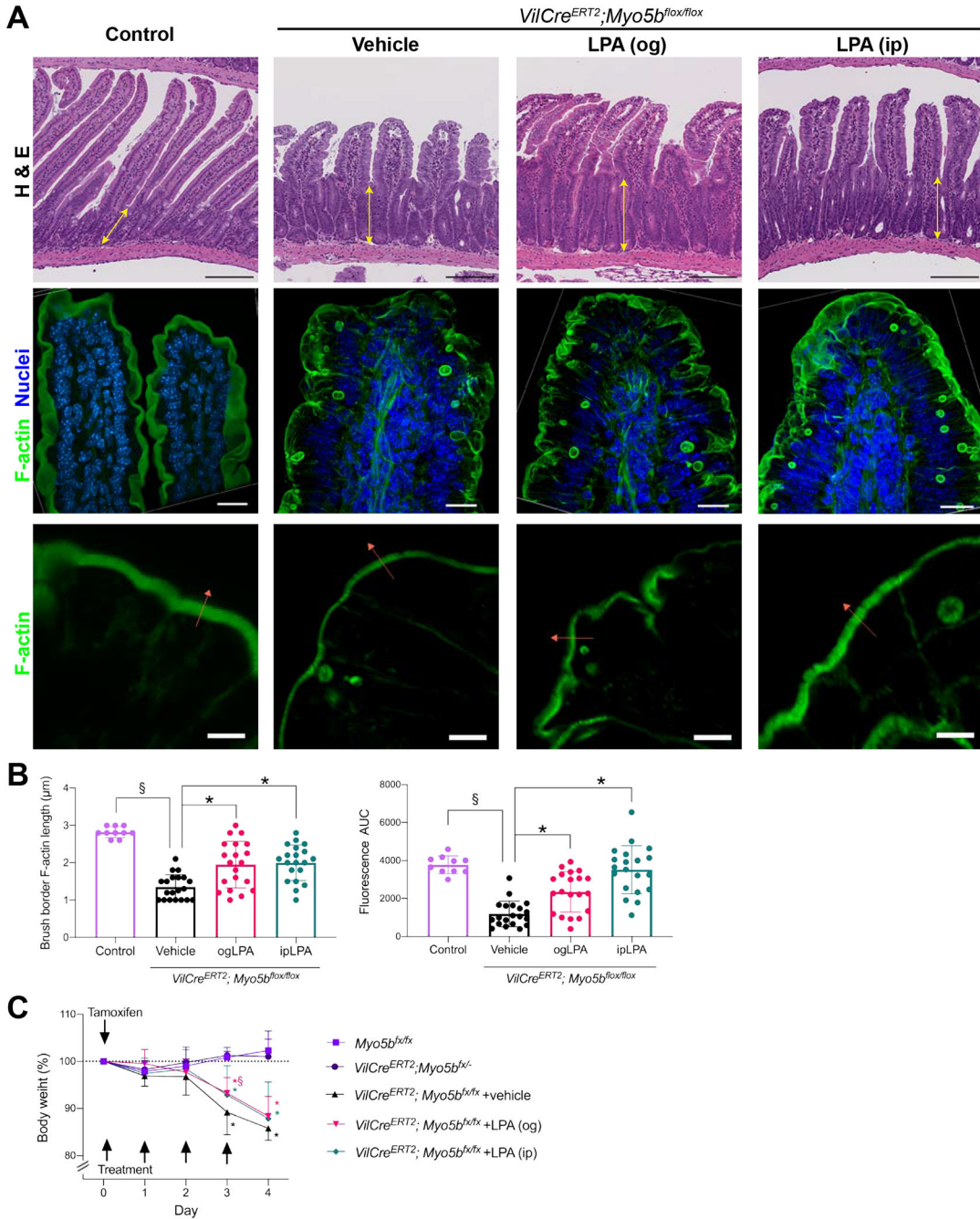
Figure 1.
Changes in body weight and jejunal morphologies by MYO5B deletion and administration of LPA in *VilCre^ERT2^;Myo5b^flox/flox^* mice. (A) Upper panel: Extended crypts (arrows) and shortened villi were observed in H&E stained paraffin sections. Scale bars = 200 μm. Middle: Three-dimensional images of frozen sections that were stained with phalloidin demonstrated thin brush border and abnormal inclusions in induced MYO5B-knockout mice. Administration of LPA improved brush border F-actin signals but not inclusion formation. Scale bars = 10 μm. Lower: Representative confocal images to measure F-actin

signals on the brush border. Arrows indicate measured sites. Scale bars = 5 μm. (B) Quantification of length and area under curve (AUC) of fluorescence across the brush border. Each datapoint represents individual measurement site. $*P < 0.01$ by Kruskal-Wallis test. (C) Relative body weight to the day of tamoxifen injection. Graph represents mean ± SD. $*P < 0.05$ *vs. Myo5b$^{flox/flox}$* and $^{§}P < 0.05$ *vs. VilCre^{ERT2}; Myo5b$^{flox/flox}$* +vehicle were detected by two-way ANOVA. $n = 5–11$ mice per group.
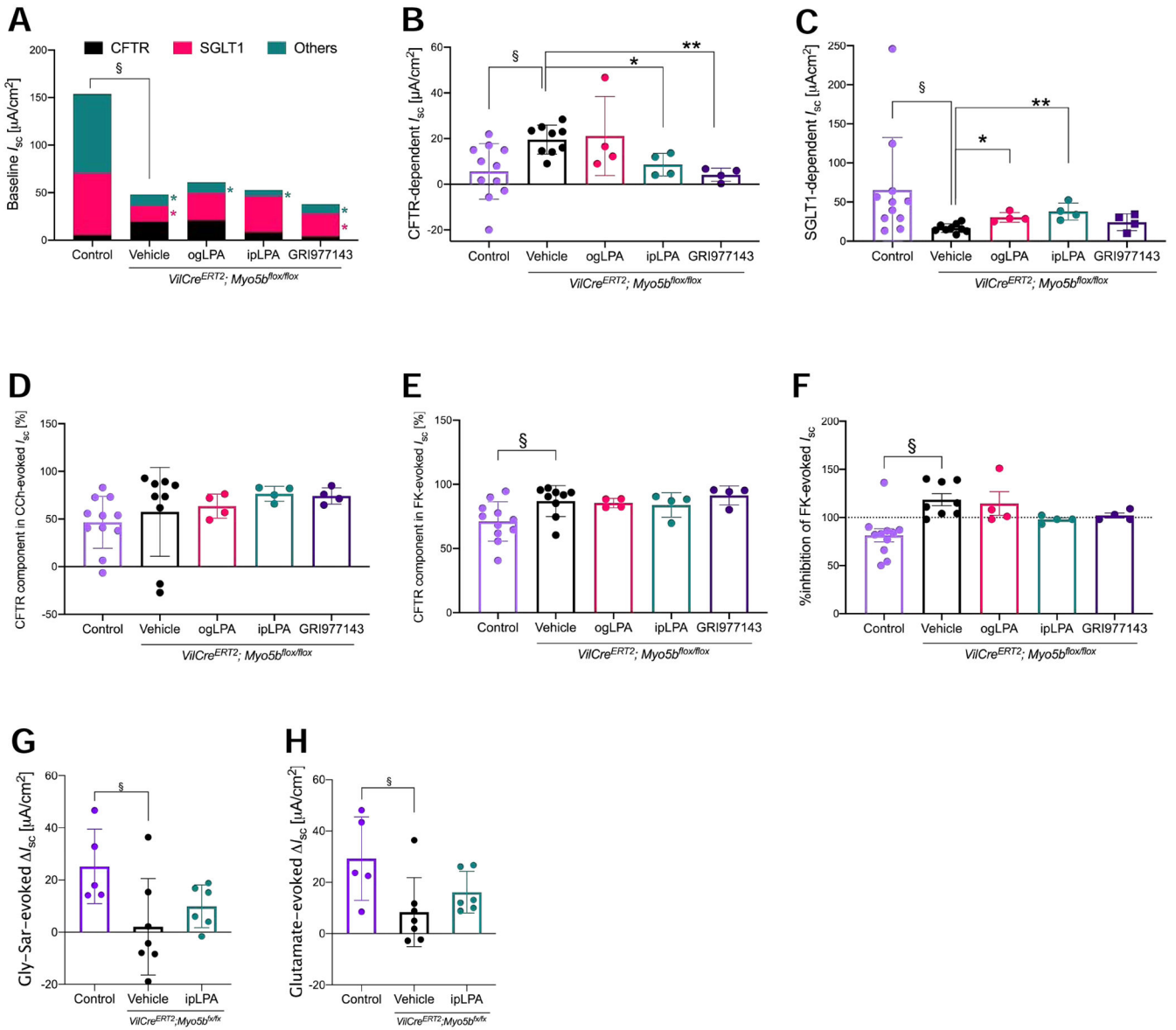
Figure 2.
Effects of administration of LPAR agonists on electrolyte transport functions in jejunum. (A) Total I_{sc} was significantly lower in MYO5B-knockout than Control. $^{§}P < 0.05$ by t-test. $^{*}P < 0.05$ by two-way ANOVA $vs.$ Control. Graph represents mean of 4 – 11 mice per group. (B and C) Basal activity of CFTR (B) and SGLT1 (C). $^{§}P < 0.05$ by t-test. $^{*}P < 0.05$ by Kruskal-Wallis test comparing drugs in MYO5B-knockout mice. (D and E) Peak values of stimulated Cl⁻ secretion were measured in the presence or absence of (R)-BPO-27, and CFTR-dependent ratio was calculated in each mouse. $^{§}P < 0.05$. (F) CFTR dependence was determined by post application of (R)-BPO-27 to the stable peak that is evoked by forskolin. $^{§}P < 0.05$. (G and H) Increases in absorptive I_{sc} were measured in response to a synthetic dipeptide glycylsarcosine (Gly-Sar) and to glutamate. $^{*}P < 0.05$ by t-test. LPA (ip) administration did not significantly increase Gly-Sar- or glutamate-induced I_{sc} (t-test).
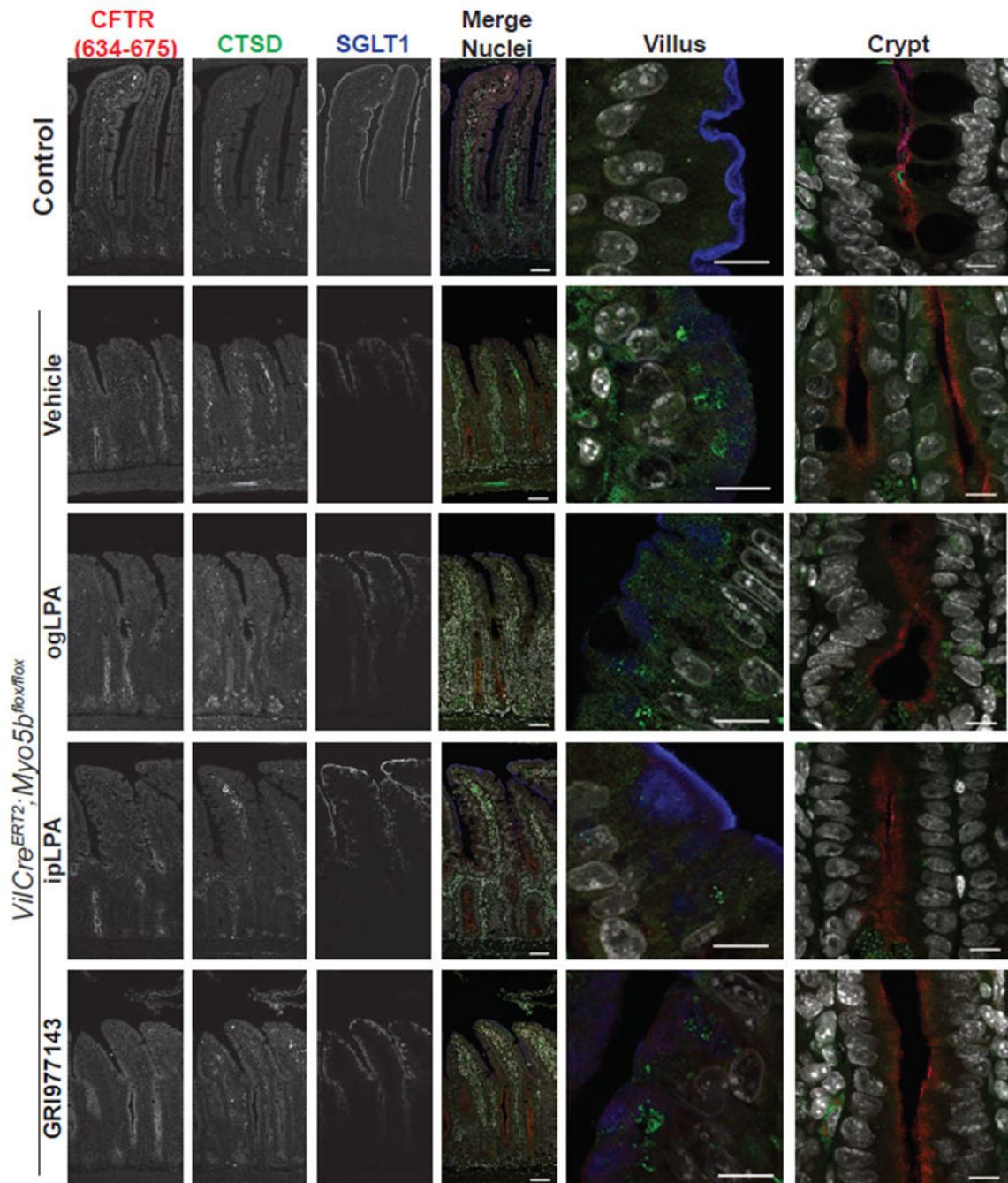
Figure 3.

Immunoreactivities for CFTR and SGLT1 together with a lysosomal protease cathepsin D (CTSD). Jejunal sections from control and LPA-given MYO5B-knockout mice were stained with antibodies against CFTR (634-675) and SGLT1(576-610). MYO5B-knockout jejunum demonstrated diffuse subapical SGLT1 (blue) and expanded cathepsin D (green) in villus cells, whereas consistent expression of CFTR (red) was observed in crypt cells. Administration of LPA, but not with the LPAR2 agonist GRI977143, partially improved

SGLT1 localization on the brush border and cathepsin D expression. Scale bar = 50 μm in merged images and 10 μm in high-magnification images.
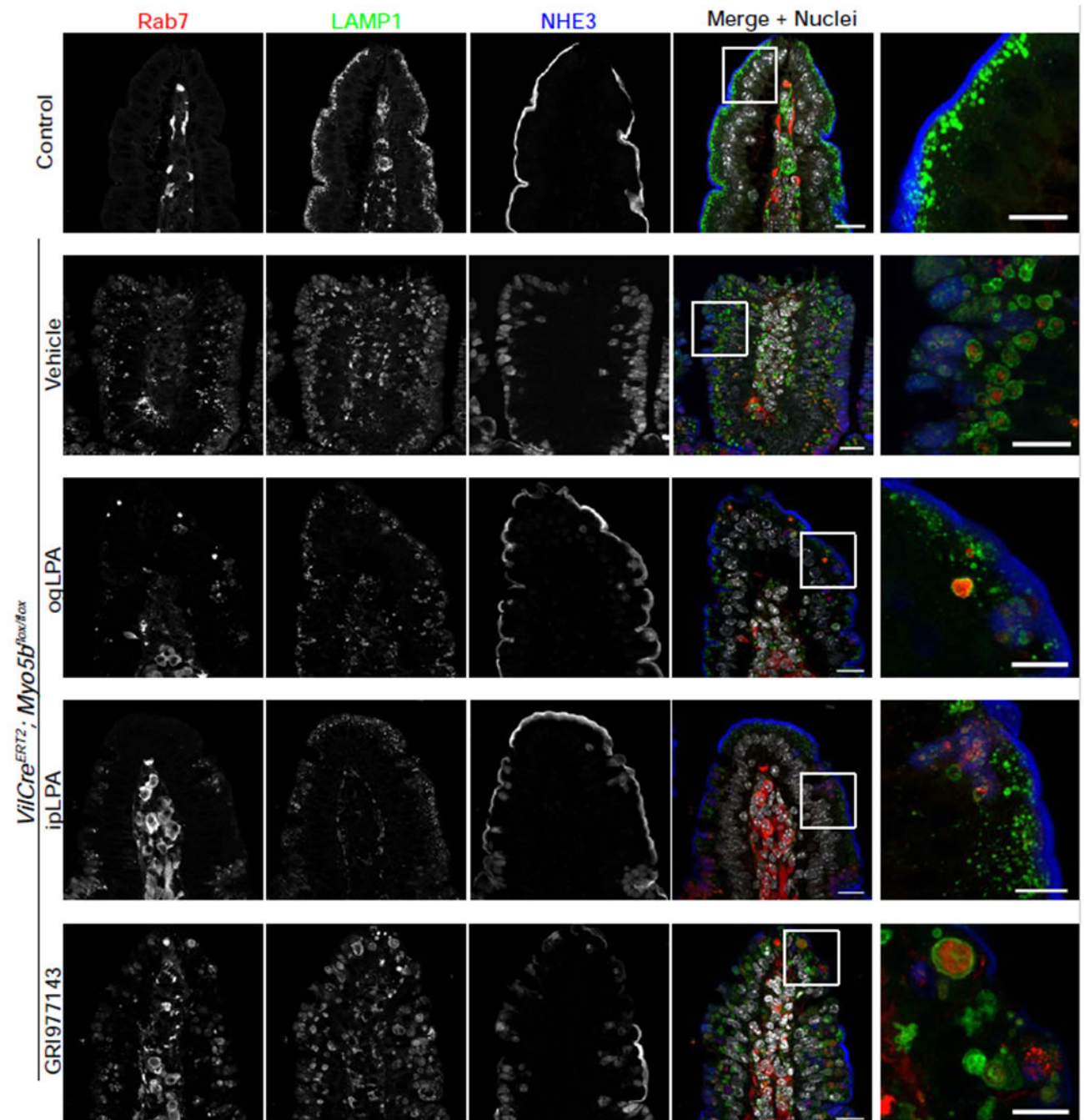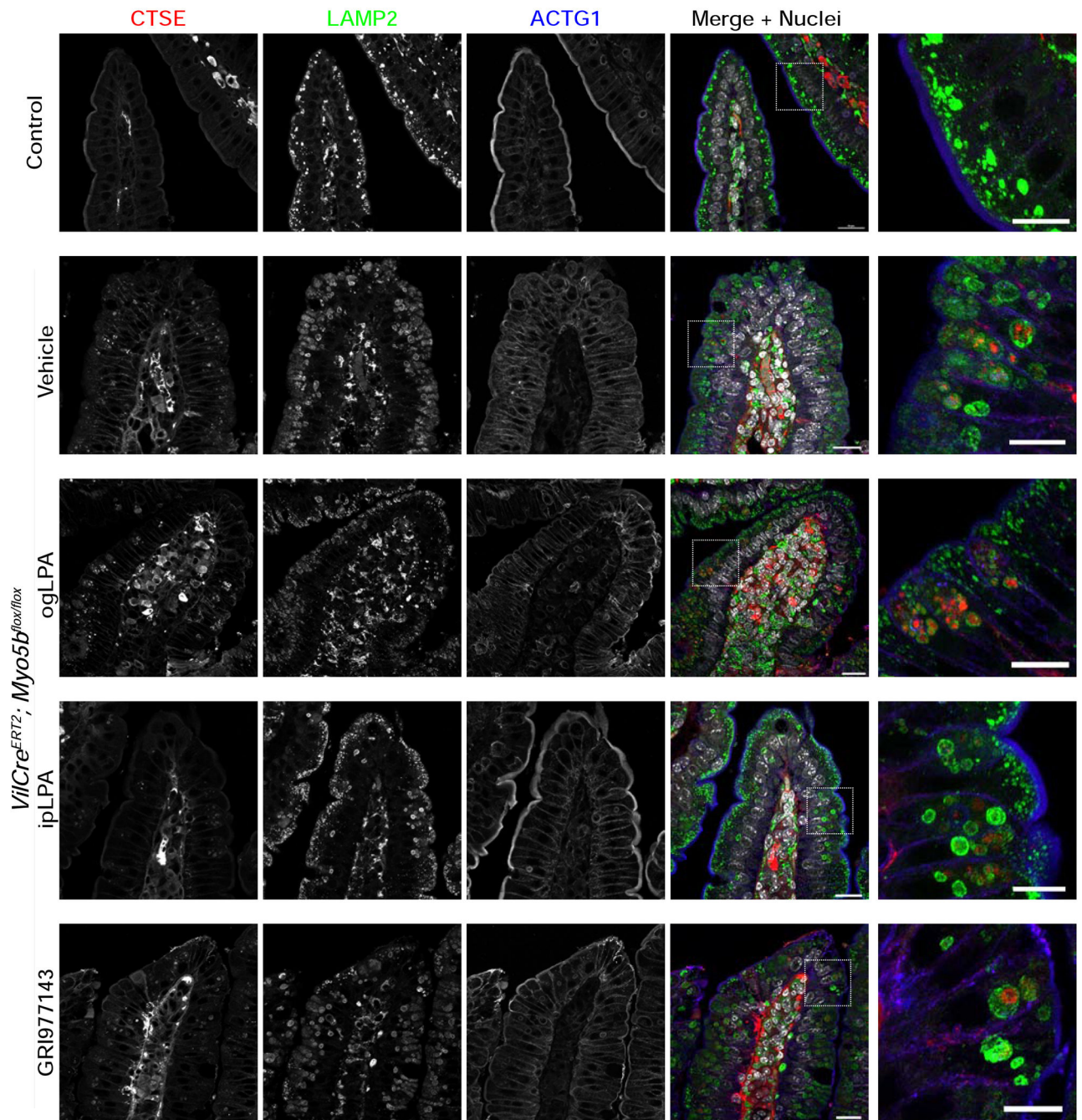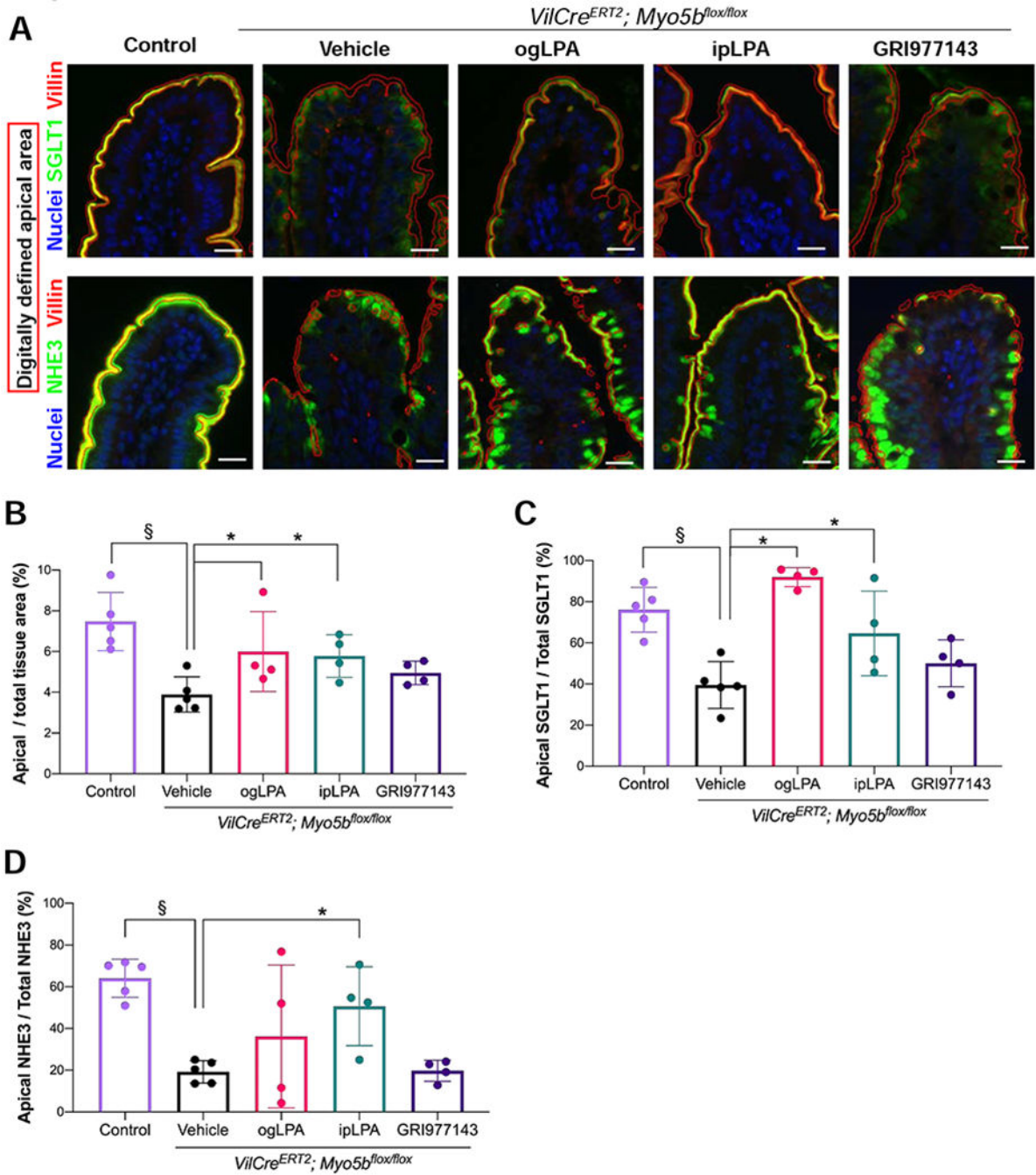
Figure 4.
Immunoreactivities for Rab7, LAMP1, and NHE3 in control and LPA-given MYO5B-knockout mice. MYO5B deficient enterocytes demonstrated Rab7 (red) expression together with expanded LAMP1 (green) in the cytoplasm and mislocalization of NHE3 (blue) from the brush border. Administration of LPA shows patchy improvement of NHE3 trafficking and normalization of lysosomal size in enterocytes. Scale bar = 20 μm in merged images and 10 μm in high-magnification images.

Figure 5.
Immunoreactivities for cathepsin E (CTSE), LAMP2, and Actg1 in control and LPA-given MYO5B-knockout mouse jejunum. Expanded LAMP2 (green)-positive lysosomes including cathepsin E (red) are frequently observed in the cytoplasm of MYO5B-knockout , but not in control tissues. Especially ip-delivered LPA administration improved cathepsin E expression and brush border structure indicated by Actg1 (red). Scale bar = 20 μm in merged images and 10 μm in high-magnification images.

Figure 6.
Apical surface area and the brush border localization of SGLT1 and NHE3 were quantified by digital image analysis of the entire jejunum. (A) Overlay images of digitally defined apical area (outlined in red) on the immunostaining for villin and SGLT1 or NHE3. Scale bar = 20 μm. (B) Ratio of digitally defined apical area in total tissue area. §$P < 0.05$ by t-test. *$P < 0.05$ by Kruskal-Wallis test with uncorrected Dunn's test. (C and D) Ratio of SGLT1 (C) or NHE3 (D) staining in apical area per total immunostained area. MYO5B loss significantly decreased the apical transporter localization and Administration of LPA

partially recovered SGLT1 and NHE3 localization. *$P < 0.05$ by ANOVA with Fisher's LSD test. Graphs show mean ± SD and each datapoint represents a mean value in each mouse.
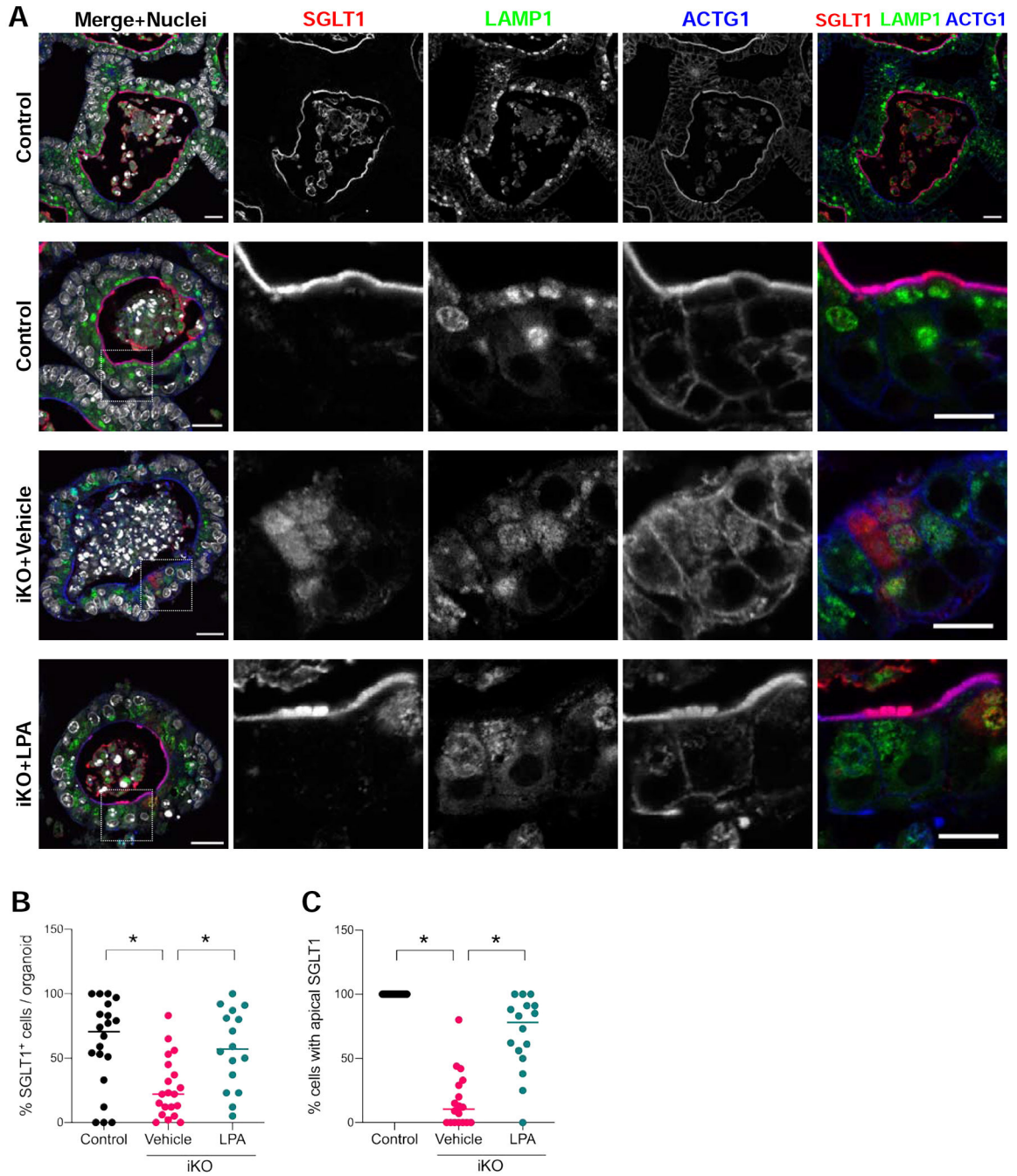
Figure 7.
Effects of LPA on the expression of SGLT1 in enteroids generated from *VilCre^ERT2;Myo5b^flox/flox* mouse jejunum. Enteroids were incubated with 4-hydroxy tamoxifen (iKO) or EtOH (Control) for 24 hours before the differentiation followed by the application of LPA or vehicle for 48 hours. (A) Immunoreactivities for SGLT1 (red), LAMP1 (green), and ACTG1 (blue) were visualized in paraffin-embedded sections. SGLT1 was mislocalized from the brush border in vehicle-treated iKO enteroids, while iKO enteroids cultured with LPA expressed SGLT1 on the brush border stained with ACTG1.

Scale bar = 20 μm in merged images and 10 μm in high magnification images. *n* = 4 mice per group. (B) Percentage of SGLT1-positive cells in each organoid section was counted. Control and LPA-supplemented iKO organoids include 60% of SGLT1-positive cells, indicating mature absorptive cells. Vehicle-treated iKO enteroids showed significantly fewer SGLT1-expresing cells. (C) Percentage of cells with brush border localization in SGLT1-positive cells was calculated. In iKO enteroids, >80% of cells did not express SGLT1 on the apical membrane, whereas LPA supplementation significantly improved SGLT1 localization. Each datapoint represents an individual organoid, and bars indicate median values. *P<0.01 by Kruskal-Wallis test.